CHEMISTRY OF MATERIALS

Article

pubs.acs.org/cm

# One-Electron Mechanism in a Gel–Polymer Electrolyte Li–$O_2$ Battery

Chibueze V. Amanchukwu,[†,‡] Hao-Hsun Chang,[§] Magali Gauthier,[§] Shuting Feng,[†] Thomas P. Batcho,[∥] and Paula T. Hammond*[,†,‡]

[†]Department of Chemical Engineering, Massachusetts Institute of Technology, Cambridge, Massachusetts 02139, United States

[‡]The David H. Koch Institute for Integrative Cancer Research, Massachusetts Institute of Technology, Cambridge, Massachusetts 02139, United States

[§]Electrochemical Energy Laboratory, Research Laboratory of Electronics, Massachusetts Institute of Technology, Cambridge, Massachusetts 02139, United States

[∥]Department of Materials Science and Engineering, Massachusetts Institute of Technology, Cambridge, Massachusetts 02139, United States

Supporting Information

**ABSTRACT:** Development of better energy storage media is vital in the adoption of renewable energy technologies, and lithium–air ($O_2$) batteries have spurred great interest. However, current Li–$O_2$ batteries are plagued by unwanted side reactions, flammable electrolytes, and slow kinetics attributed to the 2 mol $e^-$/mol $O_2$ peroxide chemistry. In this work, we show that a gel polymer electrolyte consisting of a polymer, ionic liquid, and salt can control the oxygen reduction chemistry in a Li–$O_2$ cell (switching from a 2 $e^-$ to a 1 $e^-$ superoxide chemistry), support the formation of ionic liquid–superoxide complexes, and reduce the number of reactive species present in the cell. A one electron process could allow for newer energy-dense Li–$O_2$ batteries with faster kinetics and higher energy efficiencies typical of superoxide-dominant Na–$O_2$ and K–$O_2$ batteries.

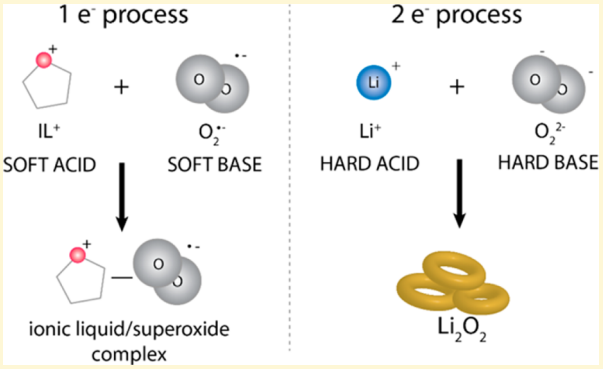


## INTRODUCTION

The need to address climate change and decrease the carbon output generated from fossil fuels has spurred rapid development and fervent commercial implementation of renewable energy technologies such as solar and wind. These energy generation technologies require the development of cheaper and more energy-dense storage media to make them viable large scale or mobile energy solutions.[1] Therefore, newer battery chemistries such as metal–air and metal–sulfur have been explored.[1−3] Among the metal–air chemistries, lithium–air ($O_2$) has the highest theoretical gravimetric energy density (~3500 Wh/$kg_{Li2O2}$),[1] and involves oxygen as the active species in combination with lithium metal.[4] Discharge of Li–$O_2$ batteries typically involves a two-electron process, where oxygen is first reduced to superoxide $O_2^{\bullet-}$ (eq 1), and further to lithium peroxide through disproportionation of lithium superoxide (a reactive free radical), (eq 3a) or an additional electrochemical reduction step (eq 3b).[4−11] On charge, it is postulated that oxidation of $Li_2O_2$ yields $Li^+$ and $O_2$ gas.[9,10,12]

$$O_2 + e^- \rightarrow O_2^{\bullet-} \quad (1)$$

$$Li^+ + O_2^{\bullet-} \rightarrow LiO_2 \quad (2)$$

$$LiO_2 + LiO_2 \rightarrow Li_2O_2 + O_2 \quad (3a)$$

$$LiO_2 + Li^+ + e^- \rightarrow Li_2O_2 \quad (3b)$$

Controlling the discharge chemistry in Li–$O_2$ cells is vital, and solvent type, catalysts, and other additives have been explored to improve the discharge capacities, current rate, and $O_2$ solubility, but have not yielded a 1 mol $e^-$/mol $O_2$ process.[8,13−15] During the writing of this paper, Lu et al. reported a 1 mol $e^-$/mol $O_2$ process in the presence of iridium nanoparticles on a reduced graphene oxide electrode in a liquid electrolyte.[16] The 2 mol $e^-$/mol $O_2$ reduction process has been suggested to be partially responsible for the kinetically limited oxygen reduction and evolution reactions, low current rates, poor capacity retention, and low cycle life typically observed in Li–$O_2$ cells.[1,4,17] In addition, conventional Li–$O_2$ batteries use nonaqueous liquid electrolytes, and their chemical and electrochemical instability,[18−20] volatility and flammability preclude their use in an oxygenated environment.

Ionic liquids (IL) and bulky cations such as tetrabutylammonium (TBA) have been shown to support a 1 mol $e^-$/mol $O_2$ process using cyclic voltammograms (CVs), but never in an actual Li–$O_2$ cell. Instead, a 2 mol $e^-$/mol $O_2$ process to form

Received: September 6, 2016
Revised: September 9, 2016
Published: September 12, 2016





DOI: 10.1021/acs.chemmater.6b03718
Chem. Mater. 2016, 28, 7167−7177

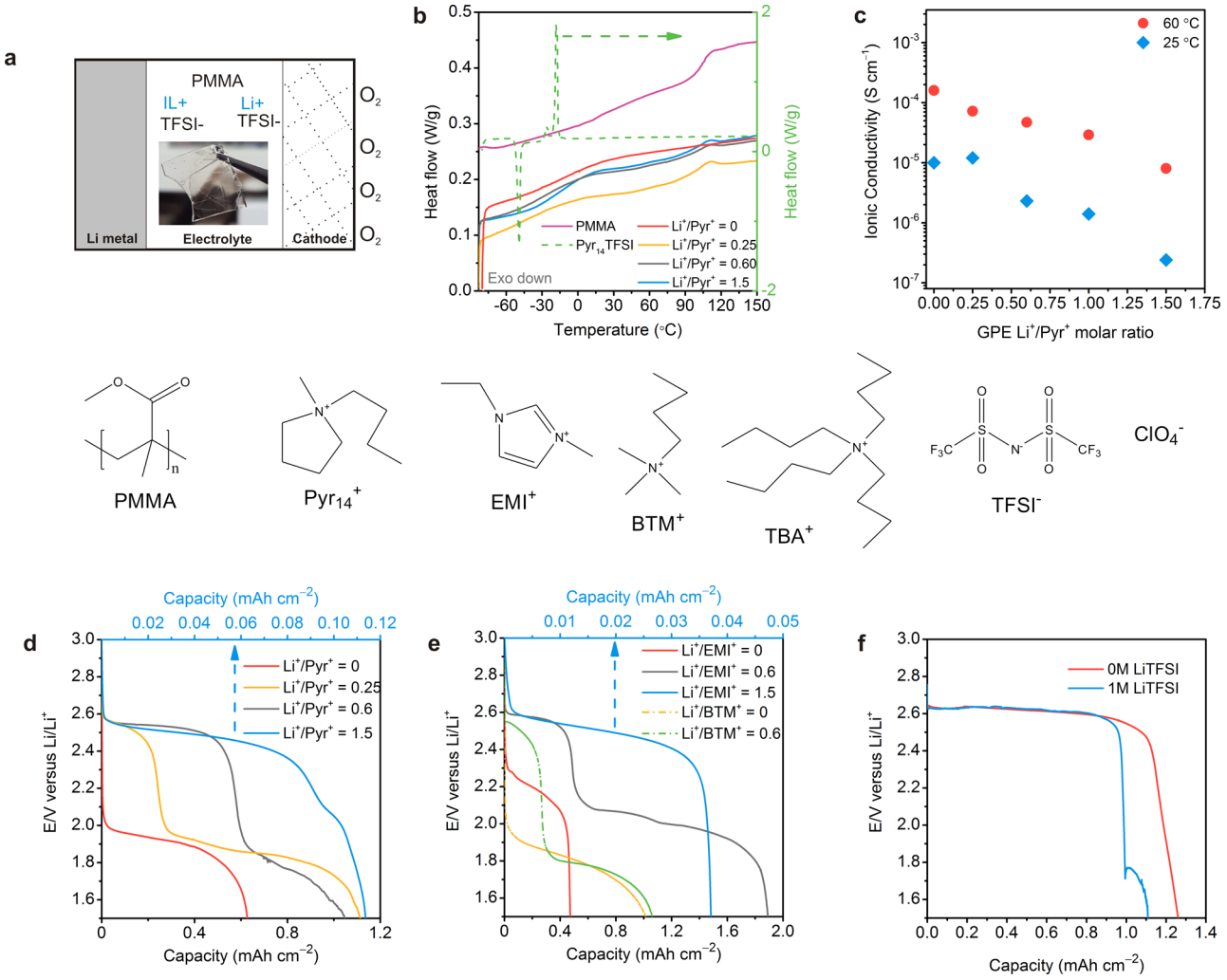


**Figure 1.** Physical and electrochemical characterization as a function of $Li^+/IL^+$ content in the GPEs and in pure ionic liquid systems (without polymer). (a) Configuration of the gel polymer electrolyte Li–$O_2$ cell. (panel a inset = flexible GPE film with $Li^+/Pyr^+$ molar ratio of 0); (b) differential scanning calorimetry (DSC) plot of PMMA, $Pyr_{14}TFSI$, and varying GPE content; (c) ionic conductivity of different GPE formulations at 25 and 60 °C; discharge curves of Li–$O_2$ cells in $O_2$ of varying $Li^+/Pyr^+$ (d) $Li^+/EMI^+$ and $Li^+/BTM^+$ (e) GPE formulations; (f) discharge curves of Li–$O_2$ cells in $O_2$ using a salt-free or 1 M LiTFSI in $Pyr_{14}TFSI$ ionic liquid electrolyte (no PMMA present in electrolyte). (d–f) Current rate = 10 $\mu A\ cm^{-2}$ (based on geometric surface area) using a Vulcan carbon/PMMA electrode (4:1 mass ratio) at 60 °C. The ratios indicate the molar ratio of $Li^+/Pyr^+$ or $Li^+/EMI^+$ or $Li^+/BTM^+$ in the GPE. Chemical structures of the polymer, salt, and ionic liquids are shown. PMMA, poly(methyl methacrylate); $Pyr_{14}$, 1-butyl-1-methylpyrrolidinium; EMI, 1-ethyl-3-methylimidazolium; BTM, butyl-trimethylammonium; TBA, tetra-*n*-butyl ammonium; TFSI, bis(trifluoromethanesulfonyl)imide. $IL^+$ = ionic liquid cation.

$Li_2O_2$ is observed when ionic liquid/salt systems based on 1-butyl-1-methylpyrrolidinium bis(trifluoromethanesulfonyl)-imide ($Pyr_{14}TFSI$) and 1-ethyl-3-methylimidazolium bis-(trifluoromethanesulfonyl)imide (EMITFSI) are used as the electrolyte in a Li–$O_2$ cell.[21] In this work, we incorporate ionic liquids into a gel polymer electrolyte (GPE), and show that the $Li^+/IL^+$ molar ratio in the GPE controls the oxygen reduction process, switching from 2 mol $e^-$/mol $O_2$ in the presence of $Li^+$ to 1 $e^-$ in the absence of $Li^+$ (and only presence of ionic liquid cation). Spectroscopic tools such as ultraviolet–visible (UV–vis) and electron paramagnetic resonance (EPR) spectroscopy were used to confirm the formation of an ionic liquid–superoxide complex not previously observed in Li–$O_2$ batteries. This discharge behavior is observed only when the ionic liquid (either ammonium, pyrrolidinium or imidazolium) is incorporated in a GPE, and not in the pure ionic liquid.

The GPE contains a polymer and an ionic liquid/lithium salt mixture, where the polymer provides mechanical support and impacts barrier and diffusion properties in the membrane, and the ionic liquid/lithium salt provides the necessary ionic conductivity. Density Functional Theory (DFT) calculations and Pearson's Hard Soft Acid Base (HSAB) theory[22] are used to explain the observed oxygen reduction phenomena, and a nonaqueous battery prototype that uses an anion-exchange membrane to simulate the GPE Li–$O_2$ cell environment is developed to demonstrate the broad scope of this work. A one electron discharge process could prove vital in alleviating the slow kinetics, poor cycle life, and reactivity concerns of standard Li–$O_2$ batteries. Moreover, the mechanism observed here could be of great interest in other metal–air and metal–sulfur batteries where controlling intermediate type and solubility is paramount.

## RESULTS AND DISCUSSION

Poly(methyl methacrylate) (PMMA) was selected as the polymer for the GPE because it was found to be stable in


DOI: 10.1021/acs.chemmater.6b03718
Chem. Mater. 2016, 28, 7167–7177

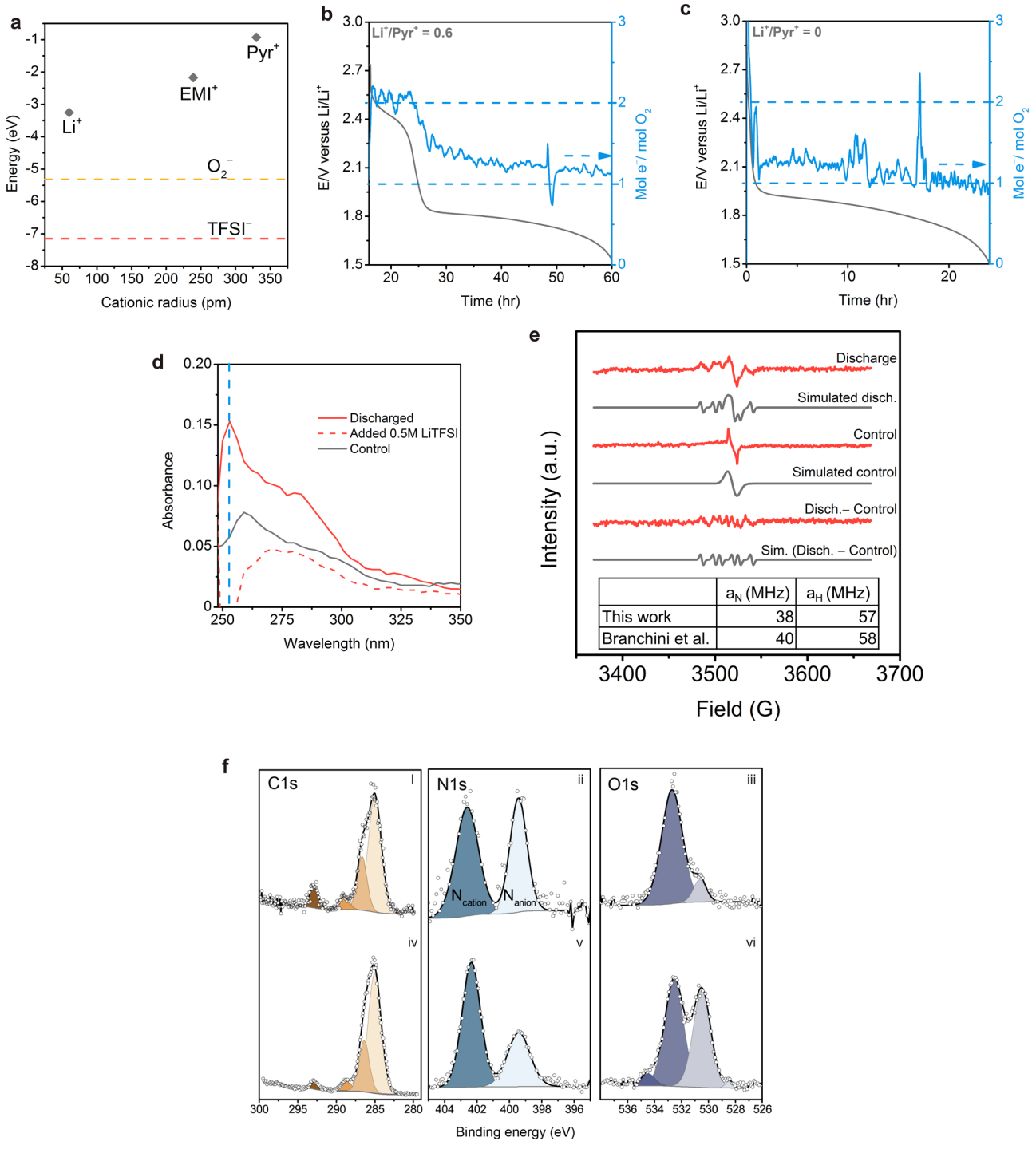


**Figure 2.** Electrochemical and spectroscopic characterization during and after the first discharge. (a) Highest occupied molecular orbital (HOMO) of superoxide and TFSI, and lowest unoccupied molecular orbital (LUMO) of respective cations as a function of cationic radius; differential electrochemical mass spectrometry (DEMS) of Vulcan carbon/$Pyr_{14}$TFSI/LiTFSI/Nafion electrode (7.8:0.7:0.5:1 mass ratio) with GPE $Li^+/Pyr^+$ molar ratio of 0.6 (b) and 0 (c) at 11.3 and 15.8 $\mu A\ cm^{-2}$ respectively (based on geometric surface area); (d) ultraviolet−visible (UV−vis) spectra of the supernatant of a discharged CNT electrode (first discharged at 10 mA $g_c^{-1}$ and then at 5 mA $g_c^{-1}$) with a GPE $Li^+/BTM^+$ molar ratio of 0 that was later soaked in dimethyl sulfoxide (DMSO), 0.5 M LiTFSI added to the discharged supernatant solution, and a control consisting of a CNT (not discharged) with a GPE $Li^+/BTM^+$ molar ratio of 0.6; (e) electron paramagnetic resonance (EPR) spectra at room temperature of the discharged CNT electrode (5 mA $g_c^{-1}$)/DMSO supernatant as in panel d with added BMPO, control as in panel d with BMPO addition. Discharge−control involves subtracting the control spectrum from the discharged spectrum. Simulated parameters are in the Methods section; panel e inset = hyperfine coupling constants for the BMPO-superoxide adduct simulated from the discharged spectra compared to the literature (ref 27); (f) XPS data chronicling the change in the C 1s, N 1s, and O 1s in the pristine (i−iii) and after 1 discharge for a CNT electrode discharged with a $Li^+/Pyr^+$ molar ratio of 0 (iv−vi). BMPO = 5-tert-butoxycarbonyl 5-methyl-1-pyrroline *N*-oxide.



DOI: 10.1021/acs.chemmater.6b03718
*Chem. Mater.* 2016, 28, 7167−7177

contact with lithium peroxide based on our finding at room temperature,[23] although a previous study reported formation of $Li_2CO_3$ in mixtures with $KO_2$. Jung et al.[24] incorporated $Pyr_{14}TFSI$ in a PVDF-HFP-based GPE in a Li−$O_2$ battery, but their films contain residual flammable *N*-methyl-2-pyrrolidone (NMP) solvent from the film fabrication process (see Supporting Information). Furthermore, PVDF-HFP undergoes extensive elimination reactions upon exposure to peroxide.[23,24] Ionic liquids with or without LiTFSI salt are incorporated within the PMMA matrix (Figure 1a) to obtain ionically conductive free-standing films with no solvent impurities (Figure S1). Although $Pyr_{14}TFSI$[25] and EMITFSI[26] are susceptible to reactions with superoxide, $Pyr_{14}TFSI$ and butyltrimethylammonium (BTM)TFSI are among the more stable ionic liquids commercially available.[26]

The $Li^+/IL^+$ molar ratio in the GPE affects the thermal properties and ionic conductivity of the GPEs. As Figure 1b shows, the amorphous PMMA prevents ordering of the ionic liquid at lower temperatures. The glass transition temperature of pure PMMA is approximately 105 °C, whereas the blends examined here show a clear suppression of this glass transition, with a small inflection appearing at approximately 20 to 30 °C instead, closer to room temperature. As lithium salt is added to the GPE, two inflections appear, one at the lower temperature and one closer to pure PMMA, implying separation of the mixture into PMMA-rich and ionic liquid/salt rich blend phases. Furthermore, the GPE content affects the net ionic conductivity where films with a $Li^+/Pyr^+$ molar ratio of 1.5 have much lower ionic conductivities ($\sim 10^{-6}$ S/cm) than films with $Li^+/Pyr^+$ molar ratios <1 ($\sim 10^{-4}$ S/cm) at 60 °C (Figure 1c and Table S1). As the $Li^+/Pyr^+$ molar ratio is reduced, more free volume is generated that can allow for ionic transport, leading to GPE conductivities that approach the conductivity of the pure ionic liquid. Although the PMMA content is similar across the films, the decrease in ionic conductivity and the brittle nature of the $Li^+/Pyr^+ = 1.5$ films are due to interactions between the PMMA carbonyl group and the lithium ions that limit ion transport.

The GPEs were incorporated in Li−$O_2$ batteries as a dual separator and electrolyte with a Vulcan carbon electrode, and Figure 1d shows that GPEs can support Li−$O_2$ discharge. All Li−$O_2$ cells discussed in this work, unless otherwise stated, were tested at 60 °C. Discharge at room temperature leads to poor discharge capacities (Figure S2). At a $Li^+/Pyr^+$ molar ratio > 1, when lithium ions are in excess (compared to $Pyr^+$) in the GPE, a single discharge plateau at 2.5 V is observed. All voltages mentioned in this work are versus $Li/Li^+$. Li−$O_2$ batteries with conventional nonaqueous liquid electrolytes show similar discharge voltages.[4] Interestingly, when $0 < Li^+/Pyr^+$ molar ratio < 1, two discharge plateaus appear at 2.5 and 1.9 V. Furthermore, reduction of the $Li^+$ content when going from $Li^+/Pyr^+$ molar ratios of 0.6 down to 0.25 decreases the capacity obtained from the 2.5 V plateau. When the $Li^+/Pyr^+$ molar ratio = 0 (no lithium salt in GPE), the 2.5 V plateau disappears and only the 1.9 V plateau is observed. Therefore, the 2.5 V plateau is a function of lithium-ion content in the electrolyte; as the $Li^+$ content increases from 0 to 0.25 to 0.6, the width (capacity) of the 2.5 V plateau increases; however, once the $Li^+/Pyr^+$ ratio is greater than one, the 1.9 V plateau is absent, and the obtained capacities are 1 order of magnitude lower. The 1.9 V plateau appears kinetically limited and is not observed at high current rates (Figure S3).

The same qualitative discharge behavior as a function of $Li^+/IL^+$ molar ratio observed with Pyr-based GPEs is also seen with EMI-based and BTM-based GPEs (Figure 1e). However, the second plateau voltage is dependent on the ionic liquid cation (1.9 V for $Pyr^+$, ~1.85 V for $BTM^+$, and ~2.1 V for $EMI^+$). The same discharge behavior as in Figure 1d is also observed in Li−$O_2$ cells even with Vulcan carbon electrodes formulated with lithium salt and ionic liquid (Figure S4). Although this discharge mechanism seems to be irrespective of the type of ionic liquid cation present in the GPE, it is not observed in a pure ionic liquid (without polymer) Li−$O_2$ cell (Figure 1f).[21] When pure $Pyr_{14}TFSI$ (no salt or polymer) or 1 M LiTFSI in $Pyr_{14}TFSI$ are used as the electrolyte with a Vulcan carbon electrode using the same current rates and conditions as the GPEs, the same discharge mechanism is observed irrespective of lithium salt content. The transport of $Li^+$ from the oxidized anode is responsible for the discharge plateau in the 0 M LiTFSI in $Pyr_{14}TFSI$ system. Therefore, the incorporation of the ionic liquid into a polymeric matrix can change the voltage where the oxygen reduction reaction occurs (discussed later).

In the GPEs studied here, the ionic liquid provides a supplementary cationic source to $Li^+$ cations and thus can alter the discharge mechanism. Allen et al.[28] postulate through cyclic voltammetry (CV) that oxygen reduction in pure ionic liquid (no $Li^+$) occurs at 1.96 and 2.1 V for $Pyr_{14}TFSI$ and EMITFSI-based cells respectively, and is associated with ionic liquid−superoxide complexation. These reduction potentials are similar to those obtained in the GPE cells when $Li^+/Pyr^+$ or $Li^+/EMI^+$ molar ratio < 1. Therefore, we hypothesize that the 1.9 V plateau for $Pyr^+$ and the 2.1−2.2 V for $EMI^+$ in GPE-based Li−$O_2$ cells is due to ionic liquid−superoxide complexation. When lithium ions originally present in the GPE become depleted at the cathode, a second plateau appears when the ionic liquid cation itself becomes the active cationic species. This lithium ion exhaustion occurs in the GPEs because the lithium transference number is much lower than the pristine ionic liquid.[29,30] This suggests that, coupled with the voltage change, the oxygen reduction chemistry changes when $Li^+$ is substituted with $IL^+$ in an actual Li−$O_2$ cell. In the absence of $Li^+$, the ionic liquid cation (either $Pyr^+$, $EMI^+$ or $BTM^+$) can act as a $Li^+$ substitute and is capable of complexing the superoxide oxygen reduction products,[28] thus explaining why discharge can occur when there is no lithium salt present in the GPE. Other metal−air chemistries such as Na−air and K−air have shown rechargeable chemistries based on stable superoxide formation and oxidation, providing lower charging overpotentials, and faster one-electron oxygen reduction kinetics.[17,31] Furthermore, the ability of the GPE to sequester the superoxide intermediate may prove interesting in limiting the solubility of polysulfides and prevent their shuttle in lithium−sulfur batteries. Ionic liquid−superoxide complexation is not observed in the pure ionic liquid Li−$O_2$ cells because lithium ions can easily migrate from the anode; but is observed in the GPE-based Li−$O_2$ cells because the PMMA acts as a diffusion barrier to actively limit the transport of $Li^+$ from the oxidized anode at least on the first discharge (allowing the ionic liquid to become the active cationic specie).

In the GPE where lithium and ionic liquid cations are present, the lithium reaction with $O_2^{\bullet-}$ (high-lying HOMO) to yield $Li_2O_2$ is energetically favored (over other ionic liquid cations) because of lithium's polarizing nature, high charge density, and low-lying LUMO (Figure 2a). Density functional theory (DFT) was used to calculate the LUMO of the ionic


DOI: 10.1021/acs.chemmater.6b03718
*Chem. Mater.* 2016, 28, 7167−7177

liquid cations. Coupled with the reported lithium LUMO,[8] the trend where $Li^+$ (−3.25 eV)[8] < $EMI^+$ (−2.17 eV) < $Pyr^+$ (−0.93 eV) corroborates the observed oxygen complexation voltage where Li−$O_2$ (2.5 V) > EMI−$O_2$ (∼2.1 V) > Pyr−$O_2$ (1.9 V).

To explain why the oxygen reduction chemistry changes when lithium ions become unavailable, we apply Pearson's HSAB reasoning provided by Laoire et al.,[6,7] where the small lithium cation (radius = 60 pm)[32] with high charge density is a hard acid and the charge stabilized bulky cations such as $EMI^+$ (239 pm),[33] $Pyr^+$ (330 pm),[34] $TBA^+$ (494 pm)[32] are soft acids. Moreover, although peroxide anion is a hard base, superoxide anion is a soft base.[6,7] Hard acids prefer to bind with hard bases, and soft acids prefer to bind with soft bases.[22] If lithium cations are present when oxygen is reduced to superoxide, the oxygen reduction process does not stop at superoxide, but continues to yield peroxide ($Li_2O_2$) (Scheme 1a). This is an overall 2 $e^-$ process (hard acid − hard base). If lithium cations are absent when oxygen is reduced to superoxide, the reduction process does not proceed to peroxide; instead the superoxide complexes with the ionic liquid cation. This is an overall 1 $e^-$ process (soft acid−soft base).

To confirm the hypothesis of a 2 $e^-$ versus 1 $e^-$ process, differential electrochemical mass spectrometry (DEMS) was performed with two electrolyte configurations ($Li^+/Pyr^+$ = 0.6 and 0). As Figure 2b shows, the first plateau at 2.5 V corresponds to a 2 mol $e^-$/mol $O_2$ process (peroxide formation). As lithium ions become unavailable at the cathode, the second plateau appears and corresponds to a ∼1.2 mol $e^-$/mol $O_2$ process (superoxide formation) at the end of discharge. This imperfect ratio (1.2 vs 1 expected) could be due to concurrent superoxide and peroxide formation, although superoxide formation is dominant. For an electrolyte with no lithium salt, a 1 mol $e^-$/mol $O_2$ process is solely observed (Figure 2c). To our knowledge, this is the first time that a superoxide-dominated discharge mechanism is demonstrated in a gel polymer Li−$O_2$ battery. Scheme 1b shows a summary of the proposed discharge mechanism for a $Li^+/Pyr^+$ = 0 GPE Li−$O_2$ cell.

Other spectroscopic tools were used to confirm further the presence of superoxide in the discharge product. Carbon nanotubes (CNTs) were used as the electrode to provide higher surface area for the discharge reaction. CNT electrodes display similar discharge behavior to Vulcan carbon electrodes (Figure S5). After a CNT electrode with a $Li^+/BTM^+$ = 0 GPE was discharged, the GPE/electrode was removed from the Li−$O_2$ cell and soaked in dry dimethyl sulfoxide (DMSO). DMSO is known to solubilize superoxide.[13] The supernatant was removed from the soaked solution and then analyzed through UV−vis spectroscopy. The UV−vis data in Figure 2d show maximum absorbance at 253 nm typically associated with the $1\pi_u \rightarrow 1\pi_g$ transition of superoxide;[25,35] supporting the 1 $e^-$ superoxide reduction process. Furthermore, when excess 0.5 M lithium salt is intentionally added to the UV−vis solution, the superoxide peak diminishes because of quick disproportionation to lithium peroxide.[13] Electron paramagnetic resonance (EPR) is also typically used to detect paramagnetic species like superoxide unambiguously.[27,36] The addition of a 5-tert-butoxycarbonyl 5-methyl-1-pyrroline *N*-oxide (BMPO) spin trap to the supernatant from a discharged CNT electrode soaked in DMSO yields EPR signal with the "doublet of triplet" feature typically observed for a BMPO−superoxide radical adduct (Figure 2e).[27] These hyperfine coupling features are not

**Scheme 1. Proposed Discharge Mechanism for Varying GPE $Li^+/Pyr^+$ Molar Ratio**[a]

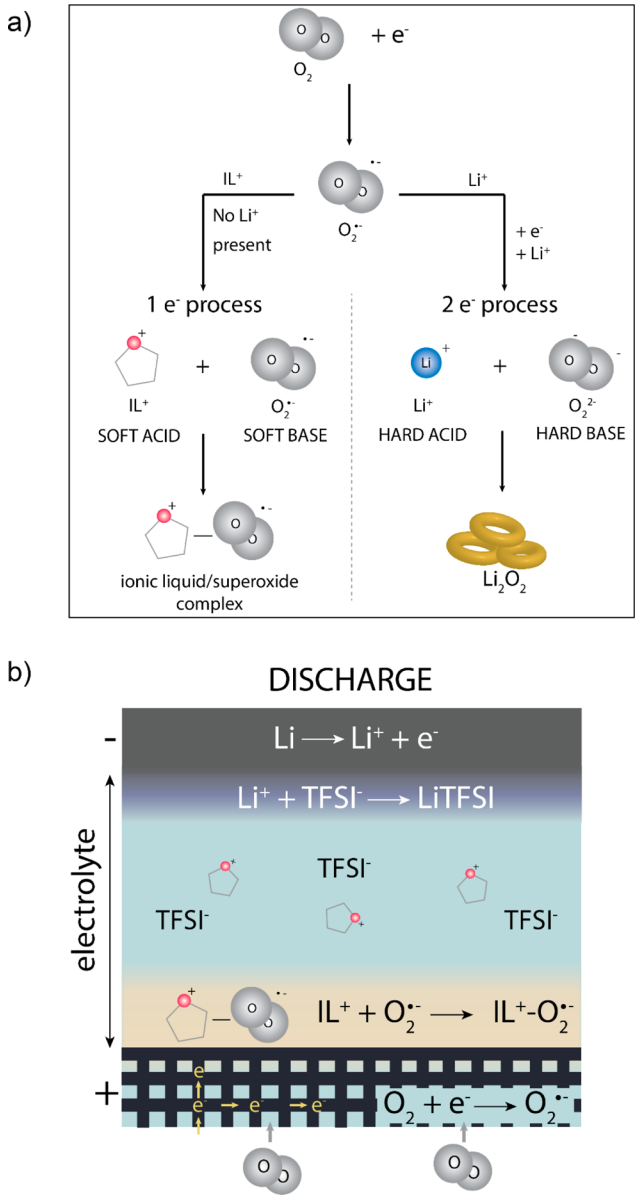


[a](a) Application of HSAB theory and the overall oxygen reduction process in the presence of $Li^+$ (2 $e^-$ process) and the absence of $Li^+$ (1 $e^-$ process in the presence of $IL^+$); (b) overall superoxide discharge mechanism when GPE $Li^+/Pyr^+$ molar ratio = 0 showing that charge neutrality is maintained. $IL^+$ = ionic liquid cation ($EMI^+$, $Pyr^+$, $BTM^+$).

observed in the control solution (CNT not discharged). Simulating the observed spectrum yields hyperfine interactions from $^{14}N$ and $^1H$ of $a_N$ = 38 MHz and $a_H$ = 57 MHz (Figure 2e) that are similar to previously reported BMPO−superoxide coupling constants of $a_N$ = 40 MHz and $a_H$ = 58 MHz,[27] further confirming the presence of superoxide in the discharged electrode.

Figure 2f shows XPS spectra that further supports the formation of a $Pyr^+-O_2^{\bullet-}$ complex. As expected, no changes are visible in the C 1s spectra from the pristine (Figure 2f (i)) to the discharged electrode (Figure 2f (iv)). However, the Nitrogen 1s peak associated with the TFSI anion[37] (binding energy = 399 eV, Figure 2f (v)) reduces compared to the $Pyr^+$



DOI: 10.1021/acs.chemmater.6b03718
Chem. Mater. 2016, 28, 7167−7177

cationic Nitrogen 1s peak[37] (B.E. = 403 eV, Figure 2f (v)), implying that the anion coordinated to the $Pyr^+$ cation has been replaced. Unsurprisingly, the O 1s spectra shows the rise of peaks at 530 and 534 eV. Several authors have attributed the peak at ~534 eV to superoxide.[38,39] Assignment of the O 1s peak at ~530 eV has been difficult and it has been attributed to superoxide[40] by some and hydroxide[41] by others. The XPS data shows that the $Pyr^+-O_2^{\bullet-}$ complex has broken the original $Pyr^+-TFSI^-$ coordination. Superoxide reaction with $Pyr^+$ can occur as observed by Schwenke et al.,[25] and is observed in XPS data obtained on another location of the same CNT electrode (Figure S6).

Scanning electron microscopy (SEM) was used to study the discharge product morphology with CNT electrodes in a GPE $Li-O_2$ cell. The pristine CNT electrodes mixed with a GPE show a coating on the CNT walls (Figure 3a,c). However,

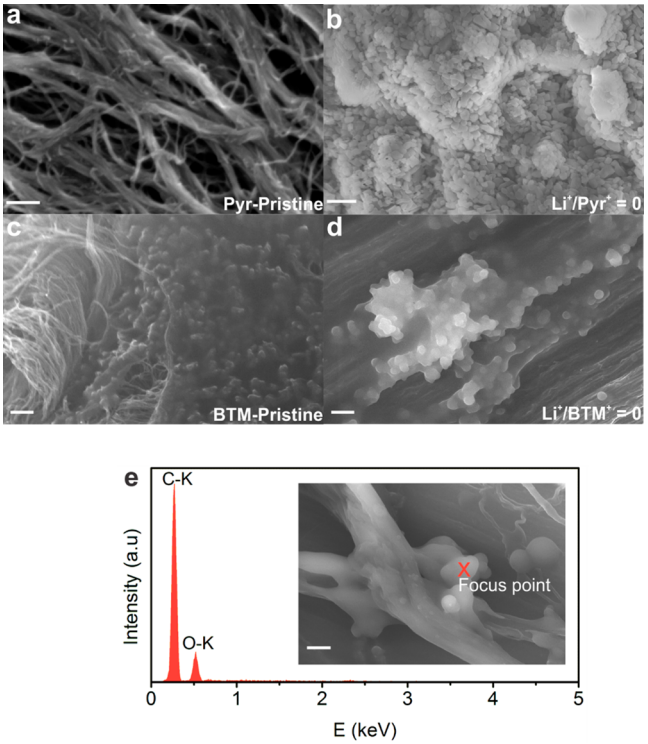


**Figure 3.** Morphology of discharged $Li-O_2$ cells using different GPE formulations. Scanning electron microscopy (SEM) images of a pristine CNT electrode sandwiched with a GPE $Li^+/Pyr^+$ (a) or GPE $Li^+/BTM^+$ (c) molar ratio of 0.6; discharged CNT electrodes with a GPE $Li^+/Pyr^+$ (b) or GPE $Li^+/BTM^+$ (d) molar ratio of 0; (e) energy dispersive spectrum (EDS) of one of the particles (shown in inset) using the same electrode in panel d. The discharged electrode in panels d and e was washed with dimethoxyethane (DME) before the SEM images were taken. The stated ratios are the molar ratio of $Li^+/Pyr^+$ or $Li^+/BTM^+$ in the GPE. CNT electrode in panel b was discharged at 10 mA $g_c^{-1}$; those in panels d and e were discharged first at 10 mA $g_c^{-1}$ and then at 5 mA $g_c^{-1}$. (a, c) scale bar = 200 nm; (b, d) scale bar = 500 nm; inset in panel e scale bar = 1 $\mu$m).

when a GPE $Li^+/Pyr^+$ molar ratio of 0 is used to support discharge, products with cuboid morphology are formed on the CNT walls (Figure 3b). These cuboids (sensitive to SEM beam damage in Figure S7) are a result of the discharge plateau below 2 V, and are reminiscent of the cubic morphology of $Na-O_2$ discharge products.[17] Similar discharge products are observed when a GPE $Li^+/BTM^+$ molar ratio of 0 is used and the observed particles grow from the CNT surface (Figure 3d). These particles in the Pyr and BTM-based cells are not present in the pristine GPE/CNT setup (Figure 3a,c), and lack the toroidal/flake-like features associated with lithium-based discharge products such as $Li_2O_2$, LiOH or $Li_2CO_3$.[18,42,43] Knowing that DEMS, UV–vis, EPR, and XPS confirms superoxide formation, and the voltage at which this superoxide complexation occurs has been verified by CV in the pure ionic liquid,[28] the cuboids observed after discharge in Figure 3b are $Pyr^+-O_2^{\bullet-}$ complexes, and the particles observed in Figure 3d–e are $BTM^+-O_2^{\bullet-}$ complexes. The energy dispersive spectrum (EDS) in Figure 3e showing C and O as the primary atomic components of the particles further supports ionic liquid–superoxide formation. The nitrogen peak is typically adjacent to the O and difficult to separate. Additional tools to determine spatially the chemical identity of the solid particles are certainly needed. The observation of these solid complexes is reminiscent of $TBA^+-O_2^{\bullet-}$ complexes that have been previously synthesized.[36] The particles are not the ionic liquid or lithium-based salts (no typical F and S anion peaks at 0.67 and 2.31 keV respectively in Figure 3e), and are not PMMA because PMMA is amorphous (Figure 1b) and should not form highly ordered particles/cuboids as observed in the SEM images. These complexes are observed using GPE-based $Li-O_2$ cells partly because limited solubility of the complex in the solid-like GPE architecture may lead to supersaturation.

When a GPE $Li^+/Pyr^+$ molar ratio of 1.5 is used, no product is observed (Figure S8) and the CNT walls are similar to the pristine (not discharged) CNT electrode (Figure 3a). This lack of discharge products is unsurprising because lower discharge capacities are obtained with a GPE molar ratio of 1.5 (Figure S5). The lower capacity is attributed to poor wetting and utilization of the cathode because of the brittle nature of the $Li^+/Pyr^+$ = 1.5 films, and the limited ionic conductivity. Reduction of the PMMA content in the $Li^+/Pyr^+$ = 1.5 GPEs should allow for more flexible films and better electrode utilization.

$Li-O_2$ cells using the PMMA-based GPEs were cycled to study their rechargeability. Figure S9 shows a $Li-O_2$ battery including a Vulcan carbon electrode cycled with $Li^+/Pyr^+$ ratios <1 and a 1.5 V cutoff, where the cell with a GPE $Li^+/Pyr^+$ ratio of 0.6 shows poor charging, and oxidation of products formed in the 1.9 V plateau does not occur. Increasing the ionic liquid content, and depressing the $Li^+/Pyr^+$ ratio to 0.25 allows for a better Coulombic efficiency (84% compared to 32%) by facilitating transport of the formed superoxide complexes to the electrode when charging begins.

To compare directly the effect of a 2 $e^-$ process versus a 1 $e^-$ process, a 2 V cutoff was used for the $Li^+/Pyr^+$ = 0.6 $Li-O_2$ cells, and a 1.5 V cutoff was used for the $Li^+/Pyr^+$ = 0 $Li-O_2$ cells. Figure 4a shows the first and fifth cycles of $Li-O_2$ cells with a GPE molar ratio of 0.6 and 0 with Vulcan carbon electrodes, and for $Li^+/Pyr^+$ = 0.6 cells, charging is reversible and mostly accomplished below 4 V. For a cell with no salt present ($Li^+/Pyr^+$ = 0), the first discharge shows a plateau just below 2 V and the charging voltages are much lower compared to the $Li^+/Pyr^+$ = 0.6 cells even at the first and fifth cycles. The second discharge plateau increases, possibly due to lithium-ion encroachment of the cathode from the oxidized anode (Figure S10). Although this $Li^+/Pyr^+$ = 0 GPE can support cycling, Coulombic efficiency at 4.5 V is 39% (first cycle); the low efficiency could be due to poor charge transfer kinetics and limited accessibility of the ionic liquid–superoxide complexes


DOI: 10.1021/acs.chemmater.6b03718
Chem. Mater. 2016, 28, 7167–7177

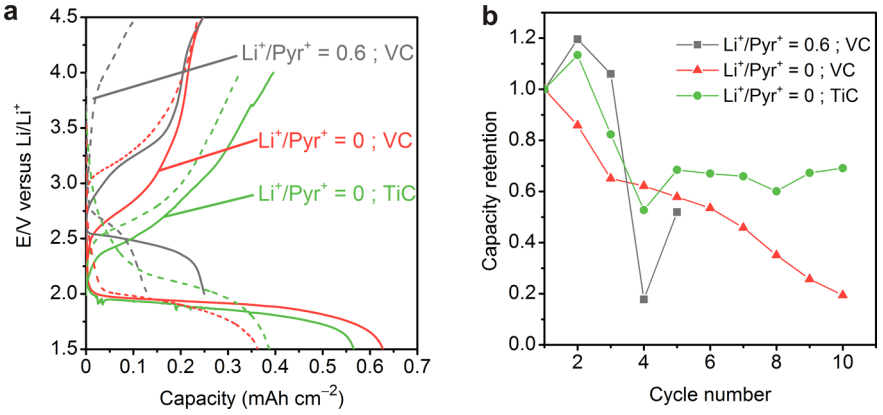


**Figure 4.** Cycling performance using different GPE formulations with different electrodes. (a) First (bold lines) and fifth cycles (dashed lines) of Vulcan carbon/PMMA electrode (4:1 mass ratio, 10 $\mu$A cm$^{-2}$) or TiC electrodes (12.4 $\mu$A cm$^{-2}$) with varying Li$^+$/Pyr$^+$ molar ratios; (b) capacity retention versus cycle number for the same Li−O$_2$ cells in panel a. A discharge cutoff of 1.5 V was used for Li$^+$/Pyr$^+$ = 0 cells, and a 2 V cutoff was used for Li$^+$/Pyr$^+$ = 0.6. Cycling performed at 60 °C and current rates based on geometric surface area.

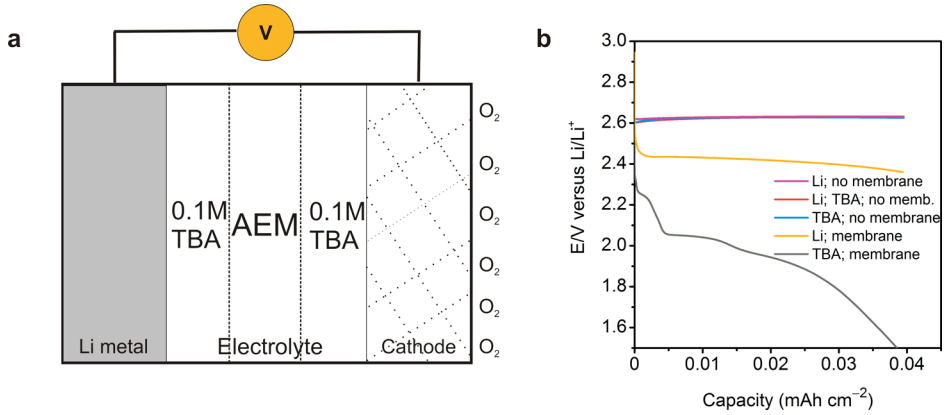


**Figure 5.** Nonaqueous Li−O$_2$ cells to mimic GPE Li−O$_2$ behavior. (a) Configuration of a Li−O$_2$ cell with an anion exchange membrane (AEM) present in a 0.1 M TBAClO$_4$ in diglyme electrolyte. (b) Discharge curves at 3.94 $\mu$A cm$^{-2}$ with different electrolyte configurations at room temperature: "Li; no membrane," "TBA; no membrane," and "Li; TBA; no memb." = electrolyte containing only 0.1 M LiClO$_4$ in diglyme, 0.1 M TBAClO$_4$ in diglyme, and a 1:2 molar mixture of LiClO$_4$:TBAClO$_4$ in diglyme, with no AEM present, respectively. "Li; membrane" and "TBA; membrane" = electrolyte containing 0.1 M LiClO$_4$ and 0.1 M TBAClO$_4$ in diglyme respectively and an AEM. Further descriptions of the legend can be found in the Supporting Information.

to the electrode. A Li$^+$/Pyr$^+$ = 1.5 GPE content was also used to show cycling for at least five cycles, and electrochemical impedance spectroscopy was used to show reversible formation and oxidation of resistive discharge products for this 2 mol e$^-$/O$_2$ process (Figure S11). Upon extensive cycling, regardless of the initial Li$^+$/Pyr$^+$ molar ratio, the cycling profiles look similar because infiltration of lithium ions from oxidized anode changes the molar balance in the GPE. The same cycling behavior observed with Li$^+$/Pyr$^+$ based cells was also observed with Li$^+$/BTM$^+$ based Li−O$_2$ cells (Figure S10).

The instability of carbon-based electrodes during Li−O$_2$ cycling[44−46] prompts the use of titanium carbide (TiC) to support Li−O$_2$ discharge and charge with different GPE formulation.[9] Similarly to the Vulcan carbon electrode in Figure 4a, the first discharge for a cell with Li$^+$/Pyr$^+$ molar ratio of 0 is below 2 V with a TiC electrode, and the fifth discharge shows a higher discharge voltage due to Li$^+$ infiltration from the oxidized anode. The charging voltages are lower compared to the Vulcan carbon electrodes, and the capacity retention even at 4 V is much better with TiC than the Vulcan carbon electrodes (Figure 4b). This electrode-dependent behavior may be due to the instability of Vulcan carbon or different electrode charge-transfer kinetics.

One benefit of this one-electron discharge mechanism is the ability to limit the number of nucleophilic species to $O_2^{\bullet-}$, and possibly prevent formation of additional reactive species like $O_2^{2-}$, $LiO_2$, and $Li_2O_2$; therefore, making the GPE Li−O$_2$ cell less prone to electrolyte degradation at least on the first cycle. GPEs recovered after multiple cycles at 60 °C show no changes in the PMMA carbonyl functionality (1700 cm$^{-1}$) in the infrared spectra, and minor decomposition products/impurities were observed in the $^1$H NMR spectra (Figure S12). Yellow coloration of the GPE, attributed to Pyr$_{14}$TFSI reduction on lithium metal,[47] was observed after discharge/cycling in Li−O$_2$ cells with GPE Li$^+$/Pyr$^+$ molar ratios <1 or when only ionic liquid was used (without polymer), but not when GPE Li$^+$/Pyr$^+$ > 1.

Finally, a prototype nonaqueous liquid Li−O$_2$ cell (Figure 5a) was developed to replicate the discharge mechanism observed in the GPE Li−O$_2$ cells. This setup is a corollary to the GPE Li−O$_2$ cell with an anion-exchange membrane (AEM) mimicking the function of the PMMA GPE by reducing free lithium-ion transport across the electrolyte, and TBA$^+$



DOI: 10.1021/acs.chemmater.6b03718
Chem. Mater. 2016, 28, 7167−7177

mimicking the ionic liquid cation ($TBAClO_4$ is dissolved in diglyme solvent). At low current rates, Figure 5b (TBA + membrane) shows that the first discharge has a plateau at around 2 V, a voltage similar to that observed for $TBA^+-O_2^{\bullet-}$ complex formation.[7] The plateau at around 2.2 V is due to $Li^+$ from the membrane (the anion for the AEM was exchanged with $LiClO_4$ prior to incorporation in the $Li-O_2$ cell; see the Experimental Section). However, when no membrane is present, irrespective of the type of salt (either $LiClO_4$ or $TBAClO_4$), a single plateau at 2.6 V is observed. Even when the membrane is used with a $LiClO_4$ electrolyte, a 2.4 V plateau is observed, further suggesting that the plateau at 2 V is not merely due to kinetic losses from membrane addition. The membrane is thus needed to limit $Li^+$ transport from the anode to enable TBA−superoxide complexation to occur and mimic the effects of the GPE. This further supports our observation in the PMMA GPE system, where superoxide complexation only occurs when lithium-ions are unavailable. Moreover, like the GPE system, only about 30% of the $TBA^+$ cations are used for superoxide complexation, resulting in low discharge capacity (see Supporting Information). Furthermore, with cycling (Figure S13), lithium ions cross the AEM, leading to higher discharge plateaus after the first discharge, again similar to the PMMA GPE-based $Li-O_2$ cells.

## ■ CONCLUSIONS

In this work, we demonstrate for the first time the use of an amorphous polymeric matrix, in combination with an ionic liquid, to control the oxygen reduction chemistry across multiple electrodes in a $Li-O_2$ cell. In the presence of Li cations, a 2 mol $e^-/O_2$ process is observed, but when $Li^+$ are absent, and ionic liquid cations are present, the ionic liquid becomes the active cationic specie, leading to a 1 mol $e^-/O_2$ process and the formation of solid ionic liquid−superoxide complexes.

The ability to obtain a 1 mol $e^-/O_2$ chemistry through a gel polymer electrolyte, without the addition of expensive catalysts, can allow for remediation of the sluggish kinetics, significant reactivity, high charging overpotentials, and poor capacity retention typically attributed to the 2 mol $e^-/O_2$ process in $Li-O_2$ batteries. Furthermore, this approach reduces the stringency of requiring high lithium-ion conductivity in electrolytes (any bulky cationic source can be used), and could be explored in other metal−air batteries, and metal−sulfur systems where the limitation of intermediate polysulfide solubility is vital. Further optimization of this system, development of more stable ionic liquids, an investigation of a broader set of stable polymer systems with differing glass transition, ionic liquid compatibility, and molecular transport properties can allow for higher ionic liquid utilization, higher capacities, and longer cycle life.

## ■ EXPERIMENTAL SECTION

**Materials.** Poly(methyl methacrylate) (Mw = 120 000), lithium bis(trifluoromethane)sulfonimide (LiTFSI) salt (99.95% trace metals basis), tetra-*n*-butylammonium perchlorate (>99.0%, for electrochemical analysis), diethylene glycol dimethyl ether (anhydrous, 99.5%), acetonitrile (anhydrous, 99.8%), dimethylformamide (anhydrous, 99.8%), deuterated dimethyl sulfoxide (DMSO) (99.9 atom % D), poly(tetrafluoroethylene) (free-flowing, 1 μm particle size), deuterated chloroform (99.8 atom % D), and isopropanol were obtained from Sigma-Aldrich. Diethylene glycol dimethyl ether (diglyme) and dimethyl sulfoxide (DMSO) were stored in 3 Å molecular sieves before use. Teflon evaporating dishes (65 mm diameter × 12 mm height) were obtained from VWR. 1-Butyl-1-methylpyrrolidinium bis(trifluoromethanesulfonyl)imide ($Pyr_{14}$TFSI, ultrapure, 99.5%), butyltrimethylammonium bis-(trifluoromethylsulfonyl)imide (BTMTFSI, 99%), and 1-ethyl-3-methylimidazolium bis(trifluoromethansulfonyl)imide (EMITFSI, ultrapure, 99.5%) were obtained from IOLITEC Inc. (Tuscaloosa, AL). Carbon paper (TGP-H-60, PTFE and non-PTFE treated) and lithium metal (0.75 mm thick, 99.9%) were obtained from Alfa Aesar. Titanium carbide (nanopowder, 99+%, 40−60 nm, cubic) was obtained from US Research Nanomaterials (Houston, TX). Nafion was obtained as a 7.2 wt % lithiated Nafion in isopropanol solution from Ion Power Inc. Celgard C480 was obtained from Celgard. Spin trap 5-tert-butoxycarbonyl 5-methyl-1-pyrroline N-oxide (BMPO) was obtained in a dimethylformamide solution from Cayman Chemical. The anion exchange membrane (Neosepta AHA) was obtained as a free sample from Ameridia (New Jersey, USA).

**Gel Polymer Electrolyte Film Fabrication.** Bohnke et al.[48] showed that in a PMMA/propylene carbonate (PC)/$LiClO_4$ GPE, a PMMA weight percentage less than 30 wt % is sufficient to retain an ionic conductivity regime similar to pure PC solvent, and also generate mechanically stable films. Therefore, unless otherwise stated, PMMA content in the PMMA/$Pyr_{14}$TFSI/LiTFSI GPEs was maintained at around 30 wt % in this study. PMMA (at least 500 mg), LiTFSI, and $Pyr_{14}$TFSI were added to a 20 mL vial in the desired amounts. Sample amounts are shown in Table S2. About 4.5 mL of acetonitrile was then added to the vial, and the mixture was stirred until a clear transparent solution was obtained. The solution was drop-casted onto a Teflon dish, and allowed to sit in a nitrogen glovebox for at least two nights to allow for evaporation of acetonitrile. Then, the Teflon dish was moved to a vacuum oven, where it was heated at 70 °C under vacuum for two more days. The films (average thickness 350−400 μm) were moved to an argon glovebox (MBRAUN, $H_2O$ < 0.1 ppm, $O_2$ < 0.1 ppm), where they were stored until use. The same procedure was used for EMITFSI-based and BTMTFSI-based GPEs. The GPE film was cut into the desired disk diameter in the glovebox just before $Li-O_2$ cell fabrication.

**Electrode Fabrication.** Several electrodes were used during this study. Vulcan carbon-based electrodes were prepared as follows: Vulcan carbon and other components, 4−5 mL of acetonitrile and 5 mm zirconia beads were added to a ball mill jar, and the contents mixed in a planetary ball mill for at least 4 h at 500 rpm. The uniform black ink was transferred onto a PTFE-treated TGP-H-60 carbon paper substrate, and a Meyer rod (RDS 60) was used to create a film. Titanium carbide (TiC) electrodes were fabricated by dispersing 90 wt % TiC and 10 wt % PTFE in isopropyl alcohol in a mortar and grinding with a pestle. The paste was then coated on nickel foam. Free-standing vertically aligned few-walled CNT carpets were fabricated as previously reported.[49] All electrodes were vacuum-dried at 75 °C before being transferred and stored in an argon glovebox (MBRAUN, $H_2O$ < 0.1 ppm, $O_2$ < 0.1 ppm).

**Ionic Conductivity Measurements.** Ionic conductivity measurements were made by sandwiching the GPE between two 15 mm stainless steel disks (Stainless steel disk | GPE | Stainless steel disk). The setup was heated at 60 °C for 10 h before electrochemical impedance spectroscopy (EIS) measurement was performed. This exact setup was allowed to rest at room temperature for 5 h before the 25 °C data point was collected. The thickness of the GPE film was determined after the EIS measurements were completed. This is because the GPE film flows during heating, leading to a different thickness before and after heating. The thickness after heating is the true thickness contributing to ionic conductivity, and is used for the calculations. The thicknesses listed in Table S1 are not the typical thickness of free-standing films that are 350−400 μm. EIS measurements were performed using a VMP3 BioLogic potentiostat in the frequency range of 1 MHz to 0.1 Hz with a signal level of 10 mV. 15 mm was used as the film diameter. The ionic conductivity values are in Table S1.

**GPE $Li-O_2$ Cell Fabrication.** Using a $Li-O_2$ cell setup developed in our laboratory,[50] lithium metal (15 mm diameter) was used as the anode, the free-standing GPE (16 mm diameter) as the electrolyte and separator, and the corresponding electrode (12.7 mm diameter for


DOI: 10.1021/acs.chemmater.6b03718
Chem. Mater. 2016, 28, 7167−7177

Vulcan carbon-based electrodes). The electrode was 80 wt % Vulcan carbon and 20 wt % PMMA. For cells using CNT carpets (1 cm × 1 cm) as the electrode, a stainless steel mesh (12.7 mm diameter) was added as the current collector. The TiC electrodes (90 wt % TiC and 10 wt % PTFE) were square pieces (12.7 mm × 12.7 mm). The cells were prepared in an argon glovebox (MBRAUN, $H_2O$ < 0.1 ppm, $O_2$ < 0.1 ppm) and moved to another Argon glovebox (MBRAUN, $H_2O$ < 0.1 ppm, $O_2$ < 0.3%), without air exposure, and filled with oxygen gas. A VMP3 potentiostat (BioLogic Inc.) was used for all electrochemical tests. The Li−$O_2$ cells were allowed to rest at 60 °C for 10 h before discharge or charge tests were performed.

For the DEMS setup, a 15 mm Li metal anode, 18 mm GPE, and 15 mm electrode (for $Li^+/Pyr^+$ = 0.6) or 12.7 mm electrode (for $Li^+/Pyr^+$ = 0) was used. The electrode was 78 wt % Vulcan carbon, 7 wt % $Pyr_{14}$TFSI, 5 wt % LiTFSI, and 10 wt % lithiated nafion on carbon paper.

**Nonaqueous Li−$O_2$ Cell Fabrication.** *Preparation of Anion Exchange Membrane.* The anion exchange membranes were cut into 18 mm disks and soaked in a 1 M $LiClO_4$ solution for two nights to allow for anion exchange. Then, the AEM disks were rinsed for 5 min with copious amounts of Milli-Q water. The AEM disks were soaked again in fresh 1 M $LiClO_4$ solution for 1 night. After rinsing again with Milli-Q water, the disks were washed with acetone before vacuum-drying at 75 °C.

The same Li−$O_2$ cell setup was used. Lithium metal (15 mm diameter) was used as the anode, two Celgard C480 membranes were used as porous separators (18 mm diameter), and a pristine TGP-H-60 (no PTFE treatment) carbon paper electrode was used for these experiments. 0.1 M $TBAClO_4$ in diglyme or 0.1 M $LiClO_4$ in diglyme or the mixture were used as stated in the main text. For cells containing the anion exchange membrane, the 18 mm AEM was sandwiched between two Celgard C480 separators. About 90 μL of electrolyte was used. Filling the cell with oxygen and testing were done as stated in the GPE Li−$O_2$ cell fabrication.

**Li−$O_2$ Fabrication with Ionic Liquid (No Polymer Present).** The same procedure for the "nonaqueous Li−$O_2$ cell fabrication" was used with Li metal anode, 90 μL of ionic liquid electrolyte, two Celgard C480 separators, and an electrode. For the 0 M LiTFSI configuration, pure $Pyr_{14}$TFSI was used as the electrolyte. An 80 wt % Vulcan carbon/20 wt % PMMA electrode on carbon paper was used. The Li−$O_2$ cell was allowed to rest at 60 °C for 10 h before discharge.

**Characterization.** *Differential Scanning Calorimetry (DSC).* 2−6 mg of PMMA, $Pyr_{14}$TFSI, and the electrolyte films were placed in hermetically sealed aluminum pans (TA Instruments). A 10 °C/min cooling and heating rate was used under a nitrogen flow rate of 50 mL/min. Two heating and cooling runs were performed on each sample to remove any thermal history. Only the second heating/cooling run is reported. A DISCOVERY DSC (TA Instruments) was used.

*Scanning Electron Microscopy (SEM).* SEM was performed using a ZEISS Merlion (Carl Zeiss Microscopy GmbH, Germany). Sample preparation was done in an argon glovebox ($O_2$ < 0.1 ppm, $H_2O$ < 0.1 ppm). For samples that were washed, the samples (Li |GPE| CNT) were placed in a 20 mL vial, and 2 mL of dimethoxyethane was added. The vial was shaken for less than 5 min until the CNT delaminated from the GPE and lithium metal. In the argon glovebox, samples were placed in an aluminum foil bag and the bag was heat sealed. The sealed foil bag was removed from the glovebox and moved to the SEM room. The sample was removed from the foil bag and in less than 5 s was transferred into the SEM chamber where high vacuum was then pulled. All images were taken with an in-lens detector at 5 kV and 68 pA. An integrated energy dispersive spectroscopy (EDAX, Ametek) instrument was used to probe the composition of the products.

*Differential Electrochemical Mass Spectrometry (DEMS).* The DEMS setup and procedure are described in ref 50.

*Ultraviolet−visible (UV−vis) Spectroscopy.* After the CNT electrode was discharged using a GPE $Li^+/BTM^+$ molar ratio of 0, the Li |GPE| CNT piece was placed in a 20 mL vial. Then, 0.3 mL of dimethyl sulfoxide was added. After 0.2 mL of the solution was removed, 0.5 mL of pure DMSO was added to the vial. Finally, 0.3 mL was removed from the vial and added to a clean 3 mL vial where it was diluted with 1 mL of DMSO. 0.01 mL of the solution in the 3 mL vial was then used for the UV−vis measurement. For the control, a Li−$O_2$ cell was made with lithium metal, a GPE $Li^+/BTM^+$ molar ratio of 0.6 and a CNT. The cell was heated at 60 °C for over 10 h, but was not discharged. The cell components were then stored in an argon glovebox for over 2 weeks. This is to ensure that the control has the same exposure with lithium metal as the discharged electrode. The cell components (Li |GPE| CNT) were then placed in a 20 mL vial. 0.3 mL of DMSO was added. 0.01 mL of the solution was then used for UV−vis measurement. These sample preparations were done in an argon glovebox. A Nano Drop ND-1000 Spectrophotometer was used in the UV−vis module and a 1 mm path. Pure DMSO was used as the blank.

*Electron Paramagnetic Resonance (EPR) Spectroscopy.* Fragments of the cell setup (either discharged or control) were added to a 3 mL vial. Then, 0.3 mL of pure DMSO was added and the vial was allowed to sit for over 4 h. 0.2 mL of the solution was removed and placed in a 1 mL vial. Then, 0.1 mL of a BMPO/dimethylformamide solution was added. The contents of the vial were mixed for a few seconds before the content was transferred to a capillary tube for EPR measurements. Sample preparations were done in an argon or nitrogen glovebox. The discharged sample and control are as described in the UV−vis spectroscopy section. Both sample and control solutions were made and characterized at the same time. EPR measurements were performed using a glass capillary tube inside a quartz tube. The spectrum was recorded on a Bruker EMS spectrometer, an ER 4199HS cavity, and a Gunn diode microwave source producing X-band radiation. Measurements were performed at room temperature with a 9.861 GHz radiation, 0.201 mW power, 100 kHz modulation frequency, and 20.48 ms time constant.

Spectral simulation was performed using the program QCMP 136 by Prof. Frank Neese from the Quantum Chemistry Program Exchange as used by Neese et al. in *J. Am. Chem. Soc.* **1996**, *118*, 8692−8699. Simulation parameters for the BMPO−superoxide adduct were obtained using a 1N, 1H model; $g_1 = g_2 = g_3 = 2.0055$ with $^{14}N$ ($a_N$ = 57 MHz) and $^1H$ ($a_H$ = 38 MHz), Gaussian line shape line broadening $W_1 = W_2 = W_3$ = 2 mT. Simulation parameters for the broad peak (originating from the control) were obtained with $g_1 = g_2 = g_3$= 2.002 and a Gaussian line shape line broadening $W_1 = W_2 = W_3$ = 6 mT.

*X-ray Photoelectron Spectroscopy (XPS) Characterization.* To avoid any exposure to air, samples were transferred from the glovebox to the XPS chamber using a sample transfer vessel (ULVAC-PHI, INC.) Spectra were collected with a PHI 5000 VersaProbe II (ULVAC-PHI, INC.) using a monochromatized Al K$\alpha$ source, a pass energy of 23.5 eV, and a charge neutralizer. All spectra were calibrated with the C 1s photoemission peak of adventitious carbon at 285 eV. Photoemission lines were fitted using combined Gaussian−Lorentzian functions after subtraction of a Shirley-type background.

*Density Functional Theory (DFT) Calculations.* All calculations were performed using the Gaussian 09 computational package. The ground state molecular structures were fully optimized in the solvent environment at the B3LYP/6-311++G(d,p) level of theory and verified by absence of any imaginary frequencies. The CPCM solvation model was used, and *N*,*N*-dimethylformamide was used as the solvent.

## ■ ASSOCIATED CONTENT

### Supporting Information

The Supporting Information is available free of charge on the ACS Publications website at DOI: 10.1021/acs.chemmater.6b03718.

Electrochemical data, ionic conductivity measurements of the GPE films, spectroscopic (NMR, FTIR, XPS) data, SEM images after cell discharge, TBA utilization calculations (PDF)



DOI: 10.1021/acs.chemmater.6b03718
*Chem. Mater.* 2016, 28, 7167−7177

## AUTHOR INFORMATION


### Corresponding Author

*P. T. Hammond. E-mail: hammond@mit.edu.


### Notes

The authors declare no competing financial interest.

## ACKNOWLEDGMENTS

This research was supported by the Samsung Advanced Institute of Technology (SAIT), and the facilities at the Koch Institute for Integrative Cancer Research. This work made use of the Shared Experimental Facilities supported in part by the MRSEC Program of the National Science Foundation under award number DMR-1419807. C.V.A. acknowledges support by the Department of Defense (DoD) through the National Defense Science and Engineering Graduate (NDSEG) Fellowship, and the GEM Fellowship. H-H.C. is in part supported by the Ministry of Science and Technology of Taiwan (102-2917-I-564-006-A1). T.P.B. was supported by the Skoltech Center for Electrochemical Energy Storage. The authors also thank Professor Yang Shao-Horn for fruitful discussion and help with reviewing the paper, Dr. Sang Bok Ma for help in fabricating the TiC electrodes, Shiyu Zhang for help with EPR measurements and analysis, and Jonathon Harding for constructing the differential electrochemical mass spectrometry (DEMS) instrument.

## REFERENCES


(1) Bruce, P. G.; Freunberger, S. A.; Hardwick, L. J.; Tarascon, J.-M. Li-O2 and Li-S Batteries with High Energy Storage. *Nat. Mater.* **2011**, *11*, 19−29.

(2) Girishkumar, G.; McCloskey, B.; Luntz, A.; Swanson, S.; Wilcke, W. Lithium− Air Battery: Promise and Challenges. *J. Phys. Chem. Lett.* **2010**, *1*, 2193−2203.

(3) Scrosati, B.; Hassoun, J.; Sun, Y.-K. Lithium-Ion Batteries. A Look into the Future. *Energy Environ. Sci.* **2011**, *4*, 3287−3295.

(4) Lu, Y.-C.; Gallant, B. M.; Kwabi, D. G.; Harding, J. R.; Mitchell, R. R.; Whittingham, M. S.; Shao-Horn, Y. Lithium−Oxygen Batteries: Bridging Mechanistic Understanding and Battery Performance. *Energy Environ. Sci.* **2013**, *6*, 750−768.

(5) Laoire, C.; Mukerjee, S.; Plichta, E. J.; Hendrickson, M. A.; Abraham, K. Rechargeable Lithium/TEGDME-LiPF6/ O2 Battery. *J. Electrochem. Soc.* **2011**, *158*, A302−A308.

(6) Laoire, C. O.; Mukerjee, S.; Abraham, K.; Plichta, E. J.; Hendrickson, M. A. Influence of Nonaqueous Solvents on the Electrochemistry of Oxygen in the Rechargeable Lithium− Air Battery. *J. Phys. Chem. C* **2010**, *114*, 9178−9186.

(7) Laoire, C. O.; Mukerjee, S.; Abraham, K.; Plichta, E. J.; Hendrickson, M. A. Elucidating the Mechanism of Oxygen Reduction for Lithium-Air Battery Applications. *J. Phys. Chem. C* **2009**, *113*, 20127−20134.

(8) Kwabi, D. G.; Bryantsev, V. S.; Batcho, T. P.; Itkis, D. M.; Thompson, C. V.; Shao-Horn, Y. Experimental and Computational Analysis of the Solvent-Dependent O2/Li+-O2− Redox Couple: Standard Potentials, Coupling Strength, and Implications for Lithium−Oxygen Batteries. *Angew. Chem.* **2016**, *128*, 3181−3186.

(9) Thotiyl, M. M. O.; Freunberger, S. A.; Peng, Z.; Chen, Y.; Liu, Z.; Bruce, P. G. A Stable Cathode for the Aprotic Li−O2 Battery. *Nat. Mater.* **2013**, *12*, 1050−1056.

(10) Peng, Z.; Freunberger, S. A.; Chen, Y.; Bruce, P. G. A Reversible and Higher-Rate Li-O2 Battery. *Science* **2012**, *337*, 563−566.

(11) McCloskey, B.; Bethune, D.; Shelby, R.; Girishkumar, G.; Luntz, A. Solvents' Critical Role in Nonaqueous Lithium−Oxygen Battery Electrochemistry. *J. Phys. Chem. Lett.* **2011**, *2*, 1161−1166.

(12) Chen, Y.; Freunberger, S. A.; Peng, Z.; Fontaine, O.; Bruce, P. G. Charging a Li−O2 Battery Using a Redox Mediator. *Nat. Chem.* **2013**, *5*, 489−494.

(13) Johnson, L.; Li, C.; Liu, Z.; Chen, Y.; Freunberger, S. A.; Ashok, P. C.; Praveen, B. B.; Dholakia, K.; Tarascon, J.-M.; Bruce, P. G. The Role of LiO2 Solubility in O2 Reduction in Aprotic Solvents and Its Consequences for Li−O2 Batteries. *Nat. Chem.* **2014**, *6*, 1091−1099.

(14) Lu, Y.-C.; Gasteiger, H. A.; Parent, M. C.; Chiloyan, V.; Shao-Horn, Y. The Influence of Catalysts on Discharge and Charge Voltages of Rechargeable Li−Oxygen Batteries. *Electrochem. Solid-State Lett.* **2010**, *13*, A69−A72.

(15) Wang, Y.; Zheng, D.; Yang, X.-Q.; Qu, D. High Rate Oxygen Reduction in Non-Aqueous Electrolytes with the Addition of Perfluorinated Additives. *Energy Environ. Sci.* **2011**, *4*, 3697−3702.

(16) Lu, J.; Lee, Y. J.; Luo, X.; Lau, K. C.; Asadi, M.; Wang, H.-H.; Brombosz, S.; Wen, J.; Zhai, D.; Chen, Z. A Lithium−Oxygen Battery Based on Lithium Superoxide. *Nature* **2016**, *529*, 377−382.

(17) Hartmann, P.; Bender, C. L.; Vračar, M.; Dürr, A. K.; Garsuch, A.; Janek, J.; Adelhelm, P. A Rechargeable Room-Temperature Sodium Superoxide (NaO2) Battery. *Nat. Mater.* **2013**, *12*, 228−232.

(18) Kwabi, D. G.; Batcho, T. P.; Amanchukwu, C. V.; Ortiz-Vitoriano, N.; Hammond, P.; Thompson, C. V.; Shao-Horn, Y. Chemical Instability of Dimethyl Sulfoxide in Lithium−Air Batteries. *J. Phys. Chem. Lett.* **2014**, *5*, 2850−2856.

(19) Freunberger, S. A.; Chen, Y.; Drewett, N. E.; Hardwick, L. J.; Bardé, F.; Bruce, P. G. The Lithium−Oxygen Battery with Ether-Based Electrolytes. *Angew. Chem., Int. Ed.* **2011**, *50*, 8609−8613.

(20) Freunberger, S. A.; Chen, Y.; Peng, Z.; Griffin, J. M.; Hardwick, L. J.; Bardé, F.; Novák, P.; Bruce, P. G. Reactions in the Rechargeable Lithium−O2 Battery with Alkyl Carbonate Electrolytes. *J. Am. Chem. Soc.* **2011**, *133*, 8040−8047.

(21) Elia, G.; Hassoun, J.; Kwak, W.-J.; Sun, Y.-K.; Scrosati, B.; Mueller, F.; Bresser, D.; Passerini, S.; Oberhumer, P.; Tsiouvaras, N.; Reiter, J. An Advanced Lithium−Air Battery Exploiting an Ionic Liquid-Based Electrolyte. *Nano Lett.* **2014**, *14*, 6572−6577.

(22) Pearson, R. G. Hard and Soft Acids and Bases. *J. Am. Chem. Soc.* **1963**, *85*, 3533−3539.

(23) Amanchukwu, C. V.; Harding, J. R.; Shao-Horn, Y.; Hammond, P. T. Understanding the Chemical Stability of Polymers for Lithium−Air Batteries. *Chem. Mater.* **2015**, *27*, 550−561.

(24) Jung, K.-N.; Lee, J.-I.; Jung, J.-H.; Shin, K.-H.; Lee, J.-W. A Quasi-Solid-State Rechargeable Lithium−Oxygen Battery Based on a Gel Polymer Electrolyte with an Ionic Liquid. *Chem. Commun.* **2014**, *50*, 5458−5461.

(25) Schwenke, K. U.; Herranz, J.; Gasteiger, H. A.; Piana, M. Reactivity of the Ionic Liquid Pyr14TFSI with Superoxide Radicals Generated from KO2 or by Contact of O2 with Li7Ti5O12. *J. Electrochem. Soc.* **2015**, *162*, A905−A914.

(26) Katayama, Y.; Onodera, H.; Yamagata, M.; Miura, T. Electrochemical Reduction of Oxygen in Some Hydrophobic Room-Temperature Molten Salt Systems. *J. Electrochem. Soc.* **2004**, *151*, A59−A63.

(27) Branchini, B. R.; Behney, C. E.; Southworth, T. L.; Fontaine, D. M.; Gulick, A. M.; Vinyard, D. J.; Brudvig, G. W. Experimental Support for a Single Electron-Transfer Oxidation Mechanism in Firefly Bioluminescence. *J. Am. Chem. Soc.* **2015**, *137*, 7592−7595.

(28) Allen, C. J.; Hwang, J.; Kautz, R.; Mukerjee, S.; Plichta, E. J.; Hendrickson, M. A.; Abraham, K. Oxygen Reduction Reactions in Ionic Liquids and the Formulation of a General ORR Mechanism for Li−Air Batteries. *J. Phys. Chem. C* **2012**, *116*, 20755−20764.

(29) Egashira, M.; Todo, H.; Yoshimoto, N.; Morita, M. Lithium Ion Conduction in Ionic Liquid-Based Gel Polymer Electrolyte. *J. Power Sources* **2008**, *178*, 729−735.

(30) Castiglione, F.; Ragg, E.; Mele, A.; Appetecchi, G. B.; Montanino, M.; Passerini, S. Molecular Environment and Enhanced Diffusivity of Li+ Ions in Lithium-Salt-Doped Ionic Liquid Electrolytes. *J. Phys. Chem. Lett.* **2011**, *2*, 153−157.

(31) Ren, X.; Wu, Y. A Low-Overpotential Potassium−Oxygen Battery Based on Potassium Superoxide. *J. Am. Chem. Soc.* **2013**, *135*, 2923−2926.




DOI: 10.1021/acs.chemmater.6b03718
*Chem. Mater.* 2016, 28, 7167−7177

(32) Paul, R.; Johar, S.; Banait, J.; Narula, S. Transference Number and Solvation Studies in Tetramethylurea. *J. Phys. Chem.* **1976**, *80*, 351−352.
(33) Fawcett, W. R.; Ryan, P. J. The Diffuse Double Layer in Ionic Liquids. *Collect. Czech. Chem. Commun.* **2009**, *74*, 1665−1674.
(34) Appetecchi, G. B.; Montanino, M.; Zane, D.; Carewska, M.; Alessandrini, F.; Passerini, S. Effect of the Alkyl Group on the Synthesis and the Electrochemical Properties of N-Alkyl-N-Methyl-Pyrrolidinium Bis (Trifluoromethanesulfonyl) Imide Ionic Liquids. *Electrochim. Acta* **2009**, *54*, 1325−1332.
(35) Yu, Q.; Ye, S. In Situ Study of Oxygen Reduction in Dimethyl Sulfoxide (Dmso) Solution: A Fundamental Study for Development of the Lithium−Oxygen Battery. *J. Phys. Chem. C* **2015**, *119*, 12236−12250.
(36) Dietzel, P. D.; Kremer, R. K.; Jansen, M. Tetraorganylammonium Superoxide Compounds: Close to Unperturbed Superoxide Ions in the Solid State. *J. Am. Chem. Soc.* **2004**, *126*, 4689−4696.
(37) Men, S.; Lovelock, K. R.; Licence, P. X-Ray Photoelectron Spectroscopy of Pyrrolidinium-Based Ionic Liquids: Cation−Anion Interactions and a Comparison to Imidazolium-Based Analogues. *Phys. Chem. Chem. Phys.* **2011**, *13*, 15244−15255.
(38) Ruckman, M.; Chen, J.; Qiu, S.; Kuiper, P.; Strongin, M.; Dunlap, B. Interpreting the near Edges of O2 and O2− in Alkali-Metal Superoxides. *Phys. Rev. Lett.* **1991**, *67*, 2533.
(39) Pedio, M.; Wu, Z.; Benfatto, M.; Mascaraque, A.; Michel, E.; Ottaviani, C.; Crotti, C.; Peloi, M.; Zacchigna, M.; Comicioli, C. Nexafs Experiment and Multiple Scattering Calculations on KO2: Effects on the Π Resonance in the Solid Phase. *Phys. Rev. B: Condens. Matter Mater. Phys.* **2002**, *66*, 144109.
(40) Kang, J.-S.; Kim, D.; Hwang, J.; Baik, J.; Shin, H.; Kim, M.; Jeong, Y.; Min, B. Soft X-Ray Absorption and Photoemission Spectroscopy Study of Superoxide Ko 2. *Phys. Rev. B: Condens. Matter Mater. Phys.* **2010**, *82*, 193102.
(41) Kozen, A. C.; Pearse, A. J.; Lin, C.-F.; Schroeder, M. A.; Noked, M.; Lee, S. B.; Rubloff, G. W. Atomic Layer Deposition and in Situ Characterization of Ultraclean Lithium Oxide and Lithium Hydroxide. *J. Phys. Chem. C* **2014**, *118*, 27749−27753.
(42) Lim, H.-K.; Lim, H.-D.; Park, K.-Y.; Seo, D.-H.; Gwon, H.; Hong, J.; Goddard, W. A., III; Kim, H.; Kang, K. Toward a Lithium−"Air" Battery: The Effect of CO2 on the Chemistry of a Lithium−Oxygen Cell. *J. Am. Chem. Soc.* **2013**, *135*, 9733−9742.
(43) Mitchell, R. R.; Gallant, B. M.; Thompson, C. V.; Shao-Horn, Y. All-Carbon-Nanofiber Electrodes for High-Energy Rechargeable Li−O 2 Batteries. *Energy Environ. Sci.* **2011**, *4*, 2952−2958.
(44) McCloskey, B.; Speidel, A.; Scheffler, R.; Miller, D.; Viswanathan, V.; Hummelshøj, J.; Nørskov, J.; Luntz, A. Twin Problems of Interfacial Carbonate Formation in Nonaqueous Li−O2 Batteries. *J. Phys. Chem. Lett.* **2012**, *3*, 997−1001.
(45) Ottakam Thotiyl, M. M.; Freunberger, S. A.; Peng, Z.; Bruce, P. G. The Carbon Electrode in Nonaqueous Li−O2 Cells. *J. Am. Chem. Soc.* **2012**, *135*, 494−500.
(46) Itkis, D. M.; Semenenko, D. A.; Kataev, E. Y.; Belova, A. I.; Neudachina, V. S.; Sirotina, A. P.; Hävecker, M.; Teschner, D.; Knop-Gericke, A.; Dudin, P.; et al. Reactivity of Carbon in Lithium−Oxygen Battery Positive Electrodes. *Nano Lett.* **2013**, *13*, 4697−4701.
(47) Piana, M.; Wandt, J.; Meini, S.; Buchberger, I.; Tsiouvaras, N.; Gasteiger, H. A. Stability of a Pyrrolidinium-Based Ionic Liquid in Li-O2 Cells. *J. Electrochem. Soc.* **2014**, *161*, A1992−A2001.
(48) Bohnke, O.; Frand, G.; Rezrazi, M.; Rousselot, C.; Truche, C. Fast Ion Transport in New Lithium Electrolytes Gelled with PMMA. 1. Influence of Polymer Concentration. *Solid State Ionics* **1993**, *66*, 97−104.
(49) Gallant, B. M.; Mitchell, R. R.; Kwabi, D. G.; Zhou, J.; Zuin, L.; Thompson, C. V.; Shao-Horn, Y. Chemical and Morphological Changes of Li−O2 Battery Electrodes Upon Cycling. *J. Phys. Chem. C* **2012**, *116*, 20800−20805.
(50) Harding, J. R.; Amanchukwu, C. V.; Hammond, P. T.; Shao-Horn, Y. Instability of Poly (Ethylene Oxide) Upon Oxidation in Lithium−Air Batteries. *J. Phys. Chem. C* **2015**, *119*, 6947−6955.


DOI: 10.1021/acs.chemmater.6b03718
*Chem. Mater.* 2016, 28, 7167−7177